Single molybdenum atom anchored on 2D Ti_2NO_2 MXene as a promising electrocatalyst for N_2 fixation

Yuwen Cheng,[a,b] Jianhong Dai,[a] Yan Song,[a,*] Yumin Zhang[b,*]

a School of Materials Science and Engineering, Harbin Institute of Technology at Weihai, 2 West Wenhua Road, Weihai, 264209, PR China

b National Key Laboratory of Science and Technology for National Defence on Advanced Composites in Special Environments, Harbin Institute of Technology, Harbin, 150001, PR China

*** Corresponding Authors**

E-mail: sy@hitwh.edu.cn (Y.S). E-mail: zhym@hit.edu.cn (Y.M.Z).

Abstract: Electrocatalysis synthesis of ammonia (NH_3) under ambient temperature is an attractive and challenging subject in chemical industry. The synthesis of NH_3 at ambient conditions requires efficient and stable eletrocatalysts with ultralow overpotential to ensure the low energy consumption and high yield of NH_3. Herein, the single transition metals (TM) atom (TM=Mo, Mn, Fe, Co, Ni, or Cu) anchored on 2D M_2NO_2 MXenes (M=Ti, V, and Cr), labeled as TM/M_2NO_2 are designed as electrocatalysts for N_2 reduction reaction (NRR) by density functional theory calculations. Results show that the bonding strength between Mo and Ti_2NO_2 is strong. The overpotential (η_{NRR}) of Mo/Ti_2NO_2 surface catalyzed NRR is estimated as low as 0.16 V via enzymatic mechanism, which is lower than that of up-to-date works. For Mo/V_2NO_2 and Mo/Cr_2NO_2 catalysts, the NRR belongs to the consecutive mechanism and enzymatic mechanism, with the corresponding η_{NRR} of 0.38V and 0.22 V, respectively. In addition, the reaction Gibbs free energy of NH_3 desorption from Mo/Ti_2NO_2 surface is only 0.12 eV. Electronic structure analysis indicates that Mo/Ti_2NO_2 shows metallic characteristics, which ensures the efficiently transferring of electrons between Mo and Ti_2NO_2. Ab initio molecular dynamics simulations indicated that Mo atom can be stably immobilized on Ti_2NO_2 substrate to prevent its aggregation into Mo clusters. Further analysis illustrates that hydrogen adsorption is not favor on Mo/Ti_2NO_2 surface. It should be avoided mixing with the extra gases such as NO_2, NO, SO_2, SO, and O_2 in N_2 source for NRR on Mo/Ti_2NO_2 surface. These predictions offer a new opportunity for electrocatalysis synthesizing of NH_3 by N_2 reduction in the future.

Introduction

NH_3 is an important carbon-free energy carrier due to it large hydrogen capacity and higher energy density.[1-4] It has been widely applied in various fields, such as fertilizers, resins, textile and dyes.[5-8] To date, the large-scale production of NH_3 mainly rely on Haber-Bosch process. However, the high reaction temperature (300~550 ℃) and pressure (100~300 atm) make this process requiring heavy energy consumption.[9-10] Recent years, encouraging by the biological N_2 fixation ($N_2+6H^++6e^-=2NH_3$) via nitrogenase under ambient conditions through multiple proton and electron transfer steps, electrochemical N_2 reduction reaction (NRR) method has appeared, which just requires atmospheric pressure and room temperature for NRR.[11-13] NRR through electrochemical makes energy consumption very low and the yield of NH_3 can be high by utilizing the N_2 in air as nitrogen source and controlling the applied voltage and the reaction conditions.[14-17] Till now, there are remain lots of challenges for electrochemical process of NRR due to the lack of efficient NRR electrocatalysts. Therefore, searching for high NRR electrocatalysts is important for electrochemical NRR industry.[15,18-23] Transition metal-based eletrocatalysts, including pure metals,[24-26] metal oxides,[27-28] polymers,[29] play an important role in eletrocatalysis and have been reported both experimentally and theoretically for electrochemical NRR. Recent years, the single atom catalysts (SACs) with efficient substrates have draw much attention where the single atom was served as active center and the substrate served as the electrical conductor.[30-32] Noble metal-based materials are efficient electrocatalysts for NRR, but the high price and the scarcity limit their large-scale applications in ammonia industry. It is desirable to find alternatives to noble metal-based materials for NRR. For example, Ling and coauthors found that single Mo atom supported on the graphitic-carbon nitride possesses highly activity for NRR (with the overpotential of 0.20 V),[33] Ji et al. reported that the overpotential of boron-interstitial (B_{int})-doped C_2N for NRR is as low as 0.15 V. [34]

For SACs, the substrate is one of key factors for NRR performance.[35,36] Ideal substrate should be able fix single atom, possess superior stability and excellent conductivity. 2D MXenes, with a general formula of $M_{n+1}X_nT_x$, where M stands for early transition metal, X stands for C or N, T_x is the surface functional groups, O*, OH* or F*, and n=1 to 3,[37-42] could be as potential as substrates in electro-chemistry due to their superior chemical stability.[43,44] For example, Pandey et al. have successfully synthesized Ag anchor on $Ti_3C_2T_x$ and found that the binding strength between Ag atom and $Ti_3C_2T_x$ MXene is strong.[45] Besides, Pt[46] and Pd[47] anchored on MXenes have been investigated in electrocatalysis. Transition metals (TMs), such as Mo is an important element in N_2 fixation at ambient conditions in biological systems.[48,49] Mo based electrocatalysts have exhibited excellent performances for NRR.[33,50-54] Gao et al. investigated TM (TM=Sc, Ti, Fe, Co

or Ni) anchored on $Ti_3C_2O_2$ MXenes as single metal electrocatalyst for NRR and revealed that different TM atoms delivered different overpotentials, ranging from 0.68 to 2.33 V.[51]

These literatures show that TM (including Mo) dispersed on MXenes surface possesses excellent NRR performances. However there are still lacks of reports about the TM (especially Mo) dispersed on M_2NO_2 MXenes for NRR. Therefore, in this work, we investigated catalytic performances of single TM (TM=Mo, Mn, Fe, Co, Ni or Cu) atom anchored on the 2D M_2NO_2 (M=Ti, V or Cr) as electrocatalysts for NRR based on the density functional theory calculations (DFT). Mo/Ti_2NO_2 standing out among studied TM/Ti_2NO_2 due to the strong binding strength between Mo and adsorbed N_2 (-1.05 eV) by side-on adsorption. Furthermore, Mo/Ti_2NO_2 exhibits an ultrahigh catalytic activity with low overpotential of NRR (η_{NRR}) of 0.16 V via enzymatic mechanism, indicating that NRR can efficiently proceed on the Mo/Ti_2NO_2 surface. Moreover, the reaction Gibbs free energy of NH_3 desorption from Mo/Ti_2NO_2 surface is 0.12 eV, ensuring the rapid removal of NH_3 from the catalyst surface. In addition, the metallic characteristics of Mo/Ti_2NO_2 guarantee the efficiency of transferring of electrons between Mo and Ti_2NO_2. Ab initio molecular dynamics simulations (AIMD) suggested that Mo atom can be stably anchored on Ti_2NO_2 substrate to prevent its aggregation into Mo clusters. Furthermore, hydrogen adsorption is not favor on Mo/Ti_2NO_2 surface. In addition, it should be avoided mixing with the extra gases such as NO_2, NO, SO_2, SO, and O_2 in N_2 source for NRR on Mo/Ti_2NO_2 surface. In a word, this work provides an opportunity for electrocatalysis synthesizing NH_3 through N_2 reduction in the future.

Computational details

All calculations were performed by using Vienna *ab initio* simulation package (VASP)[55,56] based on DFT. The generalized-gradient approximation potential[57] in the Perdew-Burke-Ernzerhof[58] was used. The projector-augmented wave[59] method was applied to describe the pseudopotentials. The electronic configurations of Mn, Fe, Co, Ni, Cu, Mo, Ti, V, Cr, O, N, F and H are [Ar]$3p^6$3$d^5$4s^2, [Ar] 3$d^6$4s^2, [Ar]3$d^7$4s^2, [Ar]3$d^8$4s^2, [Ar]3d^{10}4s^1, [Kr]$5p^5$4$d^5$4s^2, [Ar]$3d^3$4s^1, [Ar]$3p^6$3$d^4$4s^1, [Ar]$3p^6$3$d^5$4s^1, $2s^2$2p^4 , $2s^2$2p^3, $2s^2$2p^5, and $1s^2$, respectively. In all calculations, the van der Waals interaction was considered by using the empirical correction in Grimme's scheme, that is, DFT+D3.[60] The energy cutoff is set to 500 eV for all calculation cases, and gamma-centered *k* mesh is 9×9×2 for the unit cell of M_2N and M_2NT_x (M=Ti, V, Cr), and is set as 4×4×1 for N_2 adsorption and intermediate configurations. The convergence tolerance for the residual force on each atom during structural relaxation was set to 0.01 eV/Å and the energy difference between two consecutive self-consistent calculations is less than 10^{-4} eV, respectively. The

vacuum space in the z-direction (perpendicular to the surface) was larger than 20 Å to avoid the interaction for the periodic condition. The calculations of Gibbs free energy of each elemental step (ΔG) of NRR are adopted following the works of Nørskov et al.[61, 62] For each elemental step, ΔG is computed by eq (1):

$$\Delta G = \Delta E_{DFT} + \Delta E_{ZPE} - T\Delta S + eU + \Delta G_{pH} \quad (1)$$

where ΔE_{DFT} is the adsorption energy of a specific step. ΔE_{ZPE} and ΔS are the difference of zero point energies and the difference of entropy between the adsorbed state and the free-standing state, respectively, which are referred to the latest works about NRR.[50,51] The calculated values of zero point energy and the entropy are derived from the previous work.[50] T was set as room temperature, 298K in this work. eU is the contribution from the electrode potential. ΔG_{pH} is the contribution of pH, which is defined as $\Delta G_{pH} = -k_B T \ln[H^+] = pH \times k_B \ln 10$. The adsorption energy (ΔE_{DFT}) of different intermediates is calculated by

$$\Delta E_{DFT} = E_{total} - (E_{catal} + E_{adsorp}) \quad (2)$$

where E_{total} and E_{catal} are the total energies of the slab with and without intermediates. E_{adsorp} is the total energy of an isolate intermediate, such as N_2 and *NH. The η_{NRR} is determined by the potential limiting steps (PLS), corresponding to the most positive reaction Gibbs free energy (ΔG_{max}) defined as eq (3)

$$\eta_{NRR} = U_{equ} - U_{lim} \quad (3)$$

where U_{equ} is the equilibrium potential of NRR (~-0.16 V), and U_{lim} is the limiting potential, which is evaluated as $U_{lim} = -\Delta G_{max}/e$.[50] The pH is set to 0 and only the electrode potential effect is taken into account in the NRR process.

The binding energy between surface terminal and M_2NT_x is defined as eq (4)

$$E_b = \{E(M_2NT_x) - E(M_2N) - E(T_x)\}/2 \quad (4)$$

where $E(M_2CT_x)$, $E(M_2N)$, and $E(T_x)$ are the total energies of MXenes with and without T_x, and the isolated T_x, respectively.[63]

The binding energy of TM with M_2NO_2 is defined as eq (5)

$$E_b = E(TM/M_2NO_2) - E(M_2NO_2) - E(TM) \quad (5)$$

where $E(TM/M_2NO_2)$, $E(M_2NO_2)$, and $E(TM)$ are the total energies of M_2NO_2 MXenes with and without TM, and the isolated TM, respectively.[64]

Results and discussion

Basic properties of M_2N MXenes and surface terminal M_2NT_x

It is necessary to study the basic properties of M_2N MXenes and surface terminal M_2NT_x before investigating the NRR performances of TM/M_2NO_2. Although the family of M_2N MXenes is large,

to date, only small part of M_2N MXenes have been successfully synthesized by etching MAN phases, for example, Ti_2N and Ti_4N_3.[41] Besides, the V_2N and Cr_2N have been predicted synthesizing from V_2GaN and Cr_2GaN phases, respectively.[41] Therefore, in this work the M_2N and M_2NT_x MXenes (M=Ti, V, and Cr, T_x=O, F or OH) are selected to study their NRR performances. The calculated lattice parameters of M_2N, M_2NO_2, M_2NF_2 and $M_2N(OH)_2$ (M= Ti, V and Cr) are listed in Table S1. One can see that the values of parameter of *a* in M_2N are smaller than that of the corresponding M_2NT_x. Whereas, the values of parameter of *c* in M_2N are larger than that of the corresponding M_2NT_x. The c/a is smaller with the presence of surface T_x. The calculated total energies of M_2NO_2, M_2NF_2 and $M_2N(OH)_2$ and the binding energies E_b (via eq(4)) of T_x with M_2N MXenes with three different terminal styles are shown in Tables S2 and S3. It shows that M_2NO_2 has the lowest binding energy for all M=Ti, V and Cr. The adsorption of N* site with lowest free energy is the fcc site.

NRR performances of TM/Ti_2NO_2

Anchoring TM is an effective way to modulate the catalytic performances of MXenes.[65,66] There are three possible sites for TM to locate on the surface of M_2NO_2 (Figure S1): TM locates on the tops of N atom (H1 site), Ti atom (H2 site), O atom (T1 site). The most stable site for TM to occupy is the H1 site with the lowest relative energies as shown in Figure 2b and Table S4. Therefore, the TM/M_2NO_2 model, is built as O* locates in the fcc site of M_2N surface, and the anchored TM atom occupies at the H1 site of M_2NO_2 surface. The corresponding calculated binding energies (via eq (5)) are presented in Table S5. It shows that Mo/Ti_2NO_2 has the lowest binding energy (-1.71 eV) among the studied TM/M_2NO_2.

Based on above results, the catalytic activity of TM/Ti_2NO_2 for NRR is investigated. For NRR, there are two configurations, the side-on and end-on configurations. For each configuration, alternating and distal mechanisms for the end-on configuration, and enzymatic and consecutive mechanisms for the side-on configuration, respectively, are taken into account as shown in Figure 1. For distal and consecutive mechanisms, the proton-electron pairs (H^++e^-) first attack one of N atom to form a NH_3 and then attack another N atom to form second NH_3 (Figures 1b and 1d). While for alternating and enzymatic mechanisms, the H^++e^- attack two adsorbed N atoms and form NH_3 successively (Figures 1a and 1c).[29,43,44] More reaction details of the four mechanisms are provided in equations S1 to S21 (Supplementary Information). The intermediate structures of NRR on TM/Ti_2NO_2 via the end-on and side on configurations are shown in Figures S2 and S3.

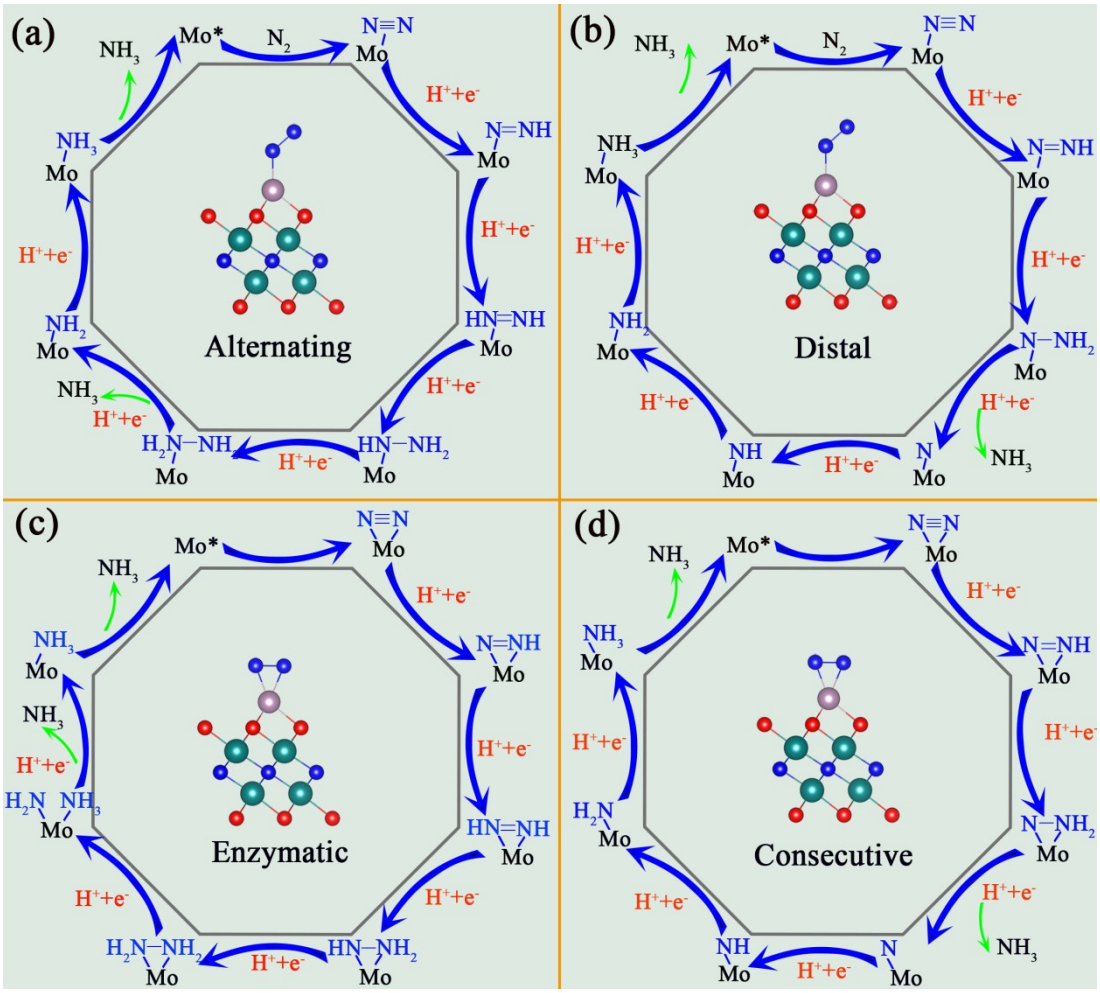

Figure 1. Schematic of (a) alternating, (b) distal, (c) enzymatic, and (d) consecutive mechanisms for N_2 reduction to NH_3 on Mo/Ti_2NO_2 surface. The * represent active sites for NRR.

Now, the NRR performances of Ti_2NO_2 and TM/Ti_2NO_2 are investigated. The reaction Gibbs free energy (ΔG) of each step through alternating, distal, enzymatic and consecutive mechanisms of TM/M_2NO_2 systems are presented in Tables S6 and S7. The calculated η_{NRR} of Ti_2NO_2 with and without TM anchored are displayed in Table S8 and Figure 2c. The ΔG diagrams for NRR on Ti_2NO_2 surface are shown in Figure S4. Results indicated that the minimum applied voltage is -2.60 V for NRR on pure Ti_2NO_2 via distal mechanism, with the corresponding η_{NRR} of 2.44 V. This ultrahigh value suggests that pure Ti_2NO_2 surface is not favor for NRR (as shown in Figure 2a). It also shows that all of NRR on TM/Ti_2NO_2 surface obey the enzymatic mechanism except Cu/Ti_2NO_2 system (which follows the alternating mechanism), and the η_{NRR} of TM/Ti_2NO_2 are lower than that of the pure Ti_2NO_2. It indicates that TM/Ti_2NO_2 promotes the NRR comparing to the pure Ti_2NO_2. More surprisingly, the superior low η_{NRR} (0.16 V) of Mo/Ti_2NO_2 is obtained, which is the lowest value among studied TM/Ti_2NO_2 systems.

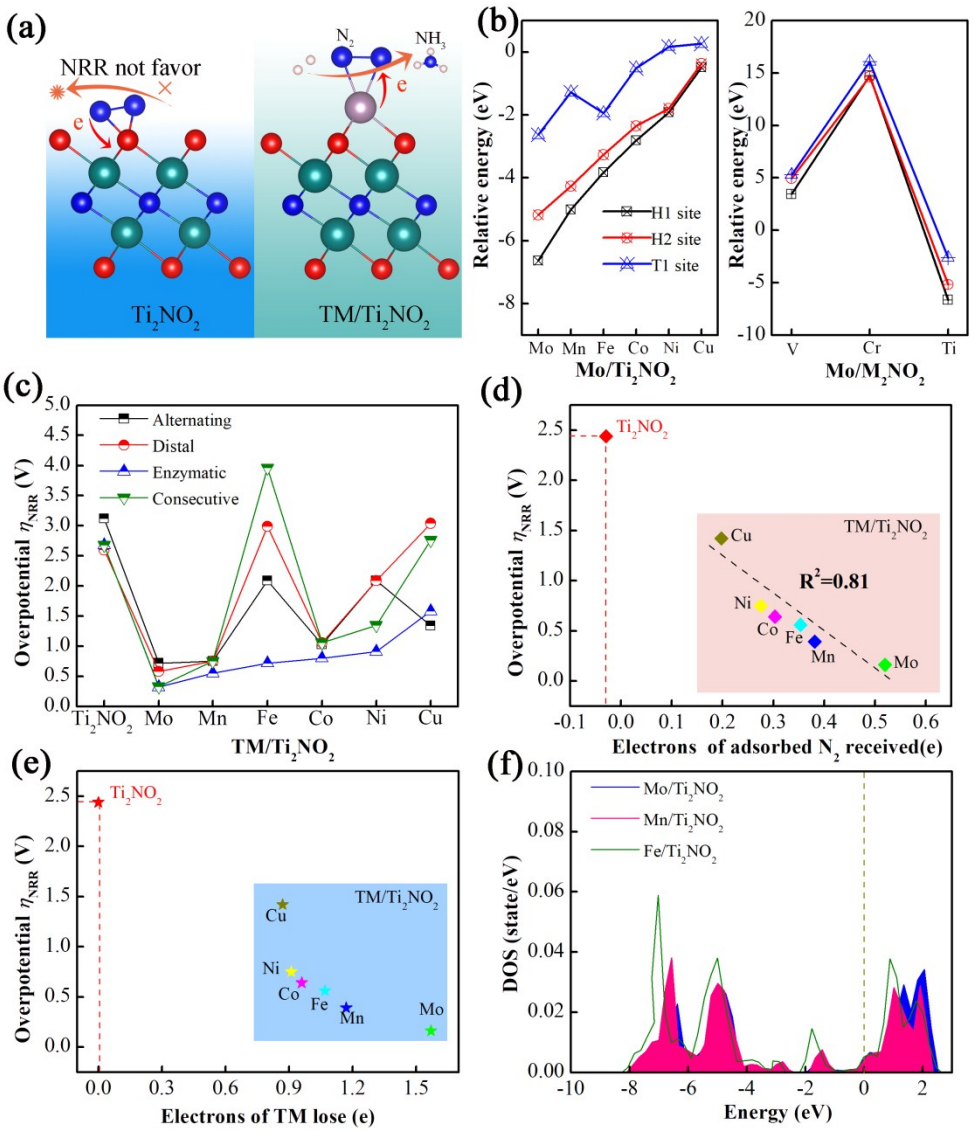

Figure 2. (a) Schematic of NRR on Ti_2NO_2 and TM/Ti_2NO_2 surface, (b) relative energies of TM/M_2NO_2 at H1, H2 and T1 sites, (c) η_{NRR} of the pure Ti_2NO_2 and TM/Ti_2NO_2 surface, (d) η_{NRR} against the electrons of adsorbed N_2 received, (e) η_{NRR} against the electrons of TM losing, and (f) densities of states of *d* orbitlal of TM (TM=Mo, Mn, and Fe).

The electrons of adsorbed N_2 received and TM losing (based on Bader charge analysis[67]) are collected and presented in Table S8. The results of η_{NRR} against the electrons of adsorbed N_2 received and TM losing are shown in Figures 2d and 2e. For the pure Ti_2NO_2 system, only 0.03 *e* electrons are transferred from the adsorbed N_2 to O*, indicating that the weak bonding strength of the O* with adsorbed N_2 and thus leads to high η_{NRR} of Ti_2NO_2 surface. The electrons transferred from TM to adsorbed N_2 increasing after TM anchored on Ti_2NO_2 surface and the electrons of adsorbed N_2 received are varied from 0.52 to 0.19 *e* in the order of Mo to Cu (Figure 2d and Table S8), while the electrons of TM losing are ranged from 1.58 to 0.87 *e* (Figure 2e), with the

corresponding values of η_{NRR} from 0.16 to 1.42 V. A linear relationship between η_{NRR} and the electrons of adsorbed N_2 received is observed with the correlation coefficient R^2 of 0.81, indicating that the NRR activity of TM/Ti_2NO_2 gradually deceases from Mo to Cu. The more electrons of TM atom losing, the higher NRR performances of TM/Ti_2NO_2 can be achieved (Figure 2e). It needs at least 6 electrons to fully drive NRR, thus more electrons of TM losing and adsorbed N_2 receiving will be more favorable to NRR. Therefore, the best NRR performances of Mo/Ti_2NO_2 among studied TM/Ti_2NO_2 ascribes to the largest electrons of Mo losing after anchored on Ti_2NO_2 surface. The calculated densities of states (DOSs) of *d* orbital of TM (TM=Mo, Mn and Fe) suggest that the *d* orbital level shifts transfer to lower energy from Mo to Fe (Figure 2f). The difference of *d* orbital occupation leads to the difference of bonding strength of TM with adsorbed N_2, and therefore causing to the various performances of NRR of TM/Ti_2NO_2.

NRR performances of Mo/M_2NO_2

Next, the NRR performances of Mo/M_2NO_2 are further evaluated. The inert N≡N triple bond is the prerequisite for an efficient NRR process.[68] Therefore the adsorption properties of N_2 on Mo/M_2NO_2 (M=Cr, V, and Ti) are first investigated. In the side-on configuration, both two N atoms bonding with Mo atom (Figure 3b), while only one of N atom interacts with Mo atom in the end-on configuration (Figure 3a). The calculated adsorption energies of N_2 adsorption through side-on and end-on configurations are listed in Table S9 with values of -1.05 and -0.94 eV, respectively, which are lower than those corresponding values in Mo/V_2NO_2 (-0.28 and -0.36 eV) and Mo/Cr_2NO_2 (-0.52 and -0.37 eV). The N≡N bond length is elongated to 1.195 (Figure 3b) and 1.140 Å (Figure 3a) compared to that of isolated N_2 molecule (1.113 Å) for side-on and end-on configurations of Mo/Ti_2NO_2, respectively. These results suggest that the N≡N triple bond can be activated once the N_2 adsorbs on the surface of Mo/M_2NO_2.

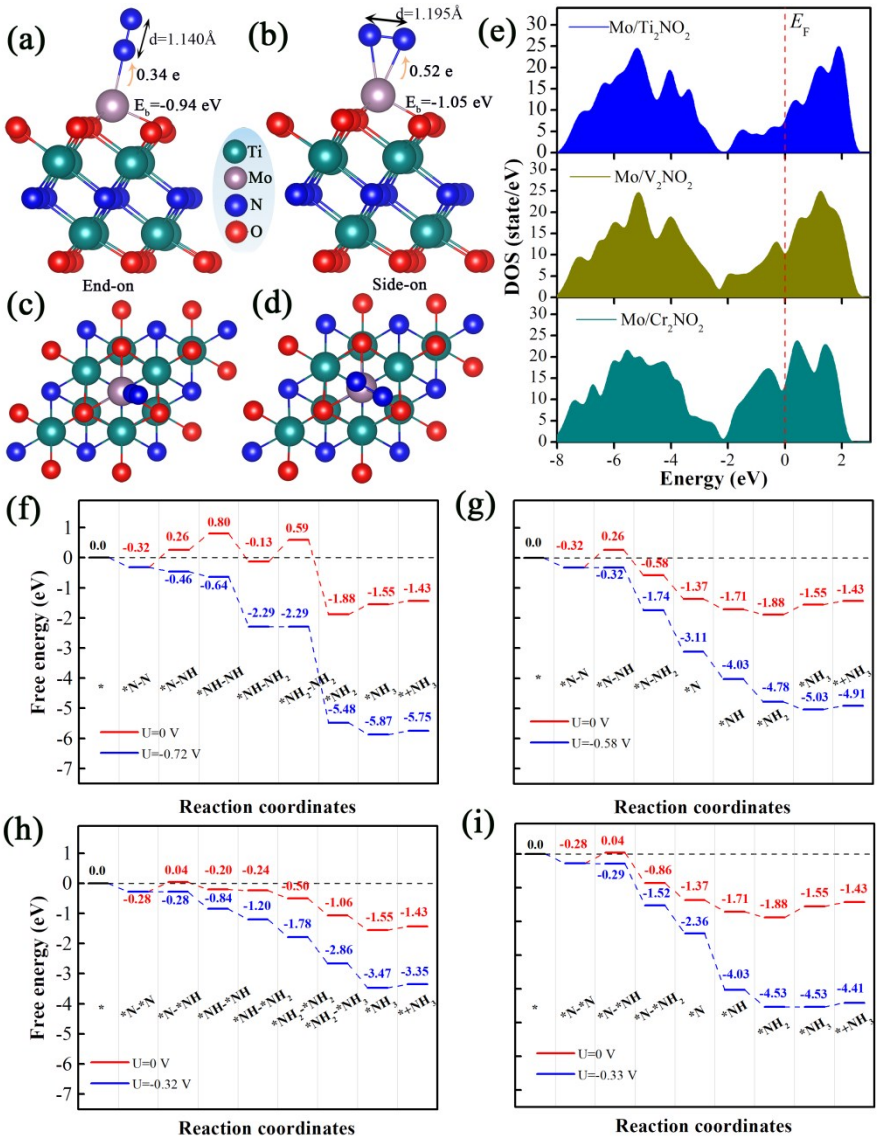

Figure 3. Adsorption of N_2 molecule on Mo/Ti_2NO_2 surface, (a) and (c) the side and top views via end-on configuration, (b) and (d) the side and top views via side-on configuration (N−N bond lengths of adsorbed N_2 and charge transfer from Mo to N_2 are also presented), (e) densities of states of Mo/M_2NO_2 (M=Ti, V, and Cr), reaction Gibbs free energy diagrams of NRR on Mo/Ti_2NO_2 through (f) alternating, (g) distal, (h) enzymatic, and (i) consecutive mechanisms under different applied potentials.

The calculated (ΔG) diagrams for NRR through alternating, distal, enzymatic and consecutive mechanisms of Mo/Ti_2NO_2 are presented in Figures 3f to 3i. The first two steps, N_2 adsorption and reduction into $*N_2H$ along the alternating and distal mechanisms are the same. The first two steps, N_2 adsorption and reduction into *NH-*N along enzymatic and consecutive mechanisms are also the same. It shows that ΔG of the first step of N_2 adsorption via end-on configuration is -0.32 eV for alternating and distal mechanisms (Figures 3f and 3g), suggesting that the N_2 molecule can be stably anchored on the Mo/Ti_2NO_2 surface. The second step of the generation of *NNH species is

endothermic with ΔG=0.58 eV. The PLS of the alternating and distal mechanisms are the *NH-NH_2 to *NH_2-NH_2 and the hydrogenation of *N_2 to *NNH with ΔG of 0.72 eV (Figure 3f) and 0.58 eV (Figure 3g), respectively. The η_{NRR} of the end-on configuration are 0.56 V (for alternating mechanism) and 0.42 V (for distal mechanism), these high η_{NRR} indicate that end-on configuration of Mo/Ti_2NO_2 is inefficient for NRR. The ΔG for N_2 adsorption via side-on configuration (for enzymatic and consecutive mechanisms) is -0.28 eV (Figures 3h and 3i). The ΔG value for the second step to generate *NH-*N via side-on pathway is 0.32 eV, which lower than the value (0.58 eV) via end-on pathway. This result reveals that the first hydrogenation step is easier via side-on pathway than that via the end-on pathway. The PLS of the enzymatic and consecutive mechanisms are the hydrogenation of *N-*N to *NH-*N and hydrogenation of *NH_2 to *NH_3, with corresponding ΔG values of 0.32 eV (Figure 3h) and 0.33 eV (Figure 3i), respectively. The η_{NRR} through enzymatic and consecutive mechanisms are 0.16 and 0.17 V, respectively. These ultra-low η_{NRR} are much lower that the best NRR catalysts,[33,50] indicating that the side-on configuration of Mo/Ti_2NO_2 possesses high catalytic activity for NRR. We also calculated the NRR performances of Mo/Ti_2NO_2 under 3×3 supercells, and results are given in Figure S5. It shows that the both of 3×3 and 2×2 supercells deliver equal overpotential, indicating that the results based on from 2×2 supercells are reliable. The calculated band structures, density of states (DOSs), and partial densities of states (pDOSs) of Mo/Ti_2NO_2 are shown in Figures 3e, S6 and S7. Result indicates that Mo/Ti_2NO_2 show metallic characteristics (Figure 3e), which will ensure efficient transfer of electrons during the NRR process. Furthermore, the DOSs near Fermi level are mainly derived from Mo *s*, *d* orbitals and O *p* orbital (Figure S7). Its indicates that the Mo promotes the transfer ability of electrons and therefore improves the NRR activity of Mo/Ti_2NO_2. The DOSs and pDOSs of Ti_2N and Ti_2NO_2 are shown in Figure S8. It shows that Ti_2N and Ti_2NO_2 are show metallic characteristics. The DOSs of Ti_2N near Fermi level are contributed from Ti *s*, *p*, and *d* orbitals. The hybridization of DOSs of Mo *d* orbital with N 2*p* orbital are further studied and shown in Figure 4. One can see that the occupation of N π*, σ and π orbitals shift to lower energy level. Moreover, the energy levels of Mo *d* orbital and N π* and σ orbitals of two N_2 adsorptions styles are matched leading to partial occupation of the d-π* and *d*-σ. Consequently, the hybridization of Mo *d* with π* and σ orbitals results in a splitting of N_2 π*: part of the π* shiting up on the Fermi level, and the other part moving down the Fermi level. The occupation of N_2 π* lowering the bond energy of N≡N triple bond, resulting the elongation of N≡N bond lengths, from 1.113 to 1.195 Å for side-on adsorption and 1.113 to 1.140 Å for end-on adsorption, with the corresponding electron gains of N atom (N_2) are 0.34 and 0.52 e, respectively. Definitety, the changes of N≡N bond lengths enhances the adsorption ability of N_2 on the Mo/Ti_2NO_2 surface.

Charge density difference of Mo/Ti_2NO_2 with adsorption of N_2 is shown in Figures 4c and d. It can be observed that the charge transfer occurred between Mo atom and adsorbed N_2 in both the side-on (Figure 4c) and end-on (Figure 4d) configurations. As it is well known, the amount of the charge transfer from one species to another relies on the relative ability of electron accepting and donating. For N_2 adsorption on Mo/Ti_2NO_2 surface, the Mo atom will donate abundant electrons to N_2 anti-bonding orbital, and then promotes the N_2 reduction.

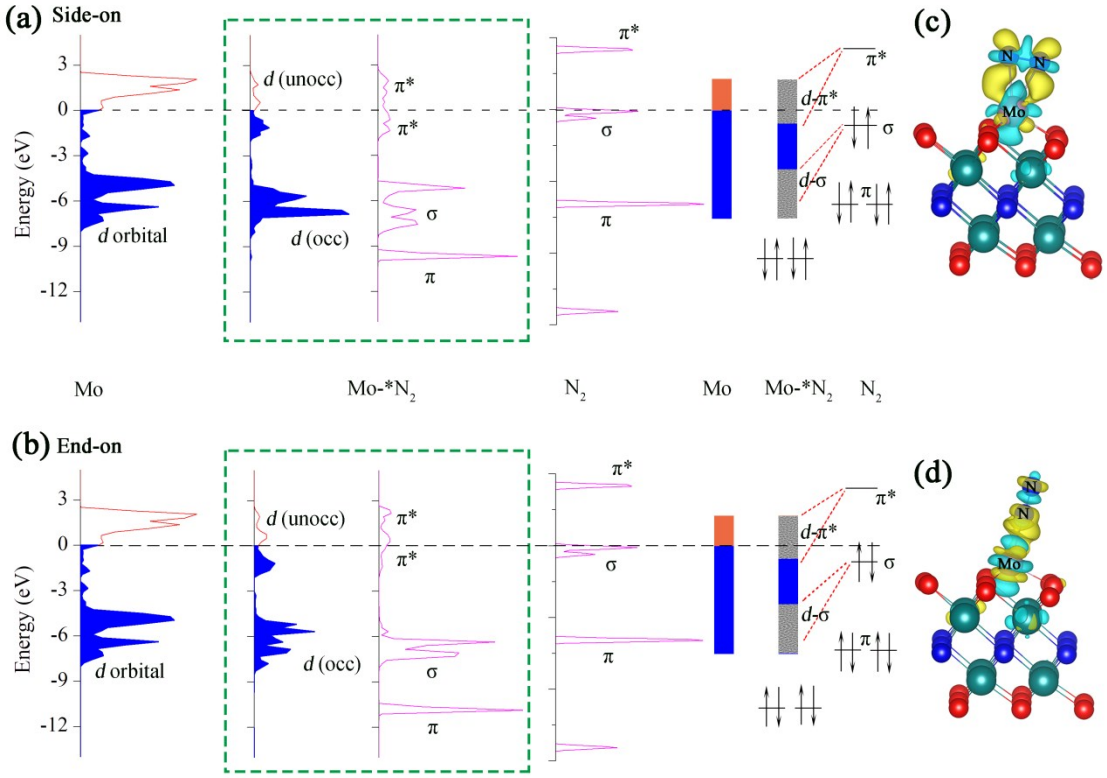

Figure 4. Projected densities of states (pDOSs) and schematic illustrations of 3*d* orbital of Mo in Ti_2NO_2, 2*p*-orbital of N_2 gas molecule, and the interaction between N_2 and Mo after N_2 adsorbed on Mo/Ti_2NO_2 surface via (a) side-on and (b) end-on configurations. Charge density difference of Mo/Ti_2NO_2 with the adsorption of N_2 via (c) end-on, and (d) side-on configurations, the positive and negative charges are shown in yellow and cyan, respectively.

For a specific NRR catalyst, the NRR performance depends not only on the ability of NRR process, but also on desorption of NH_3 from the surface of catalyst. It can be seen that ΔG for NH_3 desorption are 0.12 eV for end-on and side-on configurations (Figures 3f to 3i). Moreover, comparing with the latest NRR catalysts, Mo supported on BN[14] and V_3C_2,[69] the ΔG of NH_3 desorption are 0.92 and 0.70 eV, respectively, thus the desorption of NH_3 from Mo/Ti_2NO_2

surface are rapidly. The easy adsorption of N_2 and the rapidly desorption of NH_3 on Mo/Ti_2NO_2 surface confirm that the Mo/Ti_2NO_2 possesses the excellent NRR performances. The calculated ΔG diagrams for NRR of Mo/V_2NO_2 and Mo/Cr_2NO_2 are shown in Figures S9 and S10, respectively. It shows that Mo/V_2NO_2 and Mo/Cr_2NO_2 proceeding NRR via the enzymatic and consecutive mechanisms, respectively. The first step of N_2 molecule adsorption is exothermic, with ΔG of -0.19 for Mo/V_2NO_2 and -0.11 eV for Mo/Cr_2NO_2, respectively, while the second step (protonation) is endothermic with ΔG of 0.54 and 0.16 eV. The PLSs for Mo/V_2NO_2 and Mo/Cr_2NO_2 are the hydrogenation of *N-*N to *NH-*N and *NH_2-*NH to *NH_2-*NH_2, respectively, with the corresponding ΔG_{max} of -0.54 (Figure S9) and -0.38 eV (Figure S10), respectively. Although the calculated DOSs indicate that Mo/V_2NO_2 and Mo/Cr_2NO_2 show meallic characteristics (Figure 3e), the η_{NRR} for Mo/V_2NO_2 and Mo/Cr_2NO_2 are 0.38 V and 0.22 V, respectively, which are higher than that of Mo/Ti_2NO_2. The DOSs of M_2NO_2 MXenes are provided with considering spin-polarization (Figure S11). Similar results, metallic characteristics of M_2NO_2, could be observed. AIMD simulations were performed to simulate the stability of Mo/Ti_2CO_2, and results are given in Figure S12. It shows that the structure of Mo/Ti_2CO_2 can be stable under the NRR temperature (300K). There is another possibility that the Mo atoms will form Mo clusters (Mo_2 and Mo_9) after they are dispersed and anchored on the surface of Ti_2NO_2 due to the interaction between Mo atoms. AIMD simulations were performed to simulate the stability of Mo_2 and Mo_9 clusters on Ti_2NO_2 surface, and results are shown in Figure S13. The clusters of Mo_2 and Mo_9 are interrupted (Figures S13b, c, i, and j) when running for 1 ps. Mo tends to disperse into single isolated Mo atoms and anchored on the Ti_2NO_2 surface (bonding with O atoms) after 3ps simulation. These results illustrated that single Mo atom anchored on the Ti_2NO_2 cannot aggregate into clusters even if the temperature up to 500K. We also have studied the cohesive energy (via the definition of $E_{coh} = (E_{M(bulk)}\text{-}nE_{TM})/n$) and energy difference (ΔE_b) (via the definition of $\Delta E_b = E_b\text{-}E_{coh}$) between E_b and E_{coh}.[70] Results shows that ΔE_b of Mo/Ti_2NO_2 is -0.41 eV, indicating that the single Mo atom can be stably anchored on Ti_2NO_2 substrate.

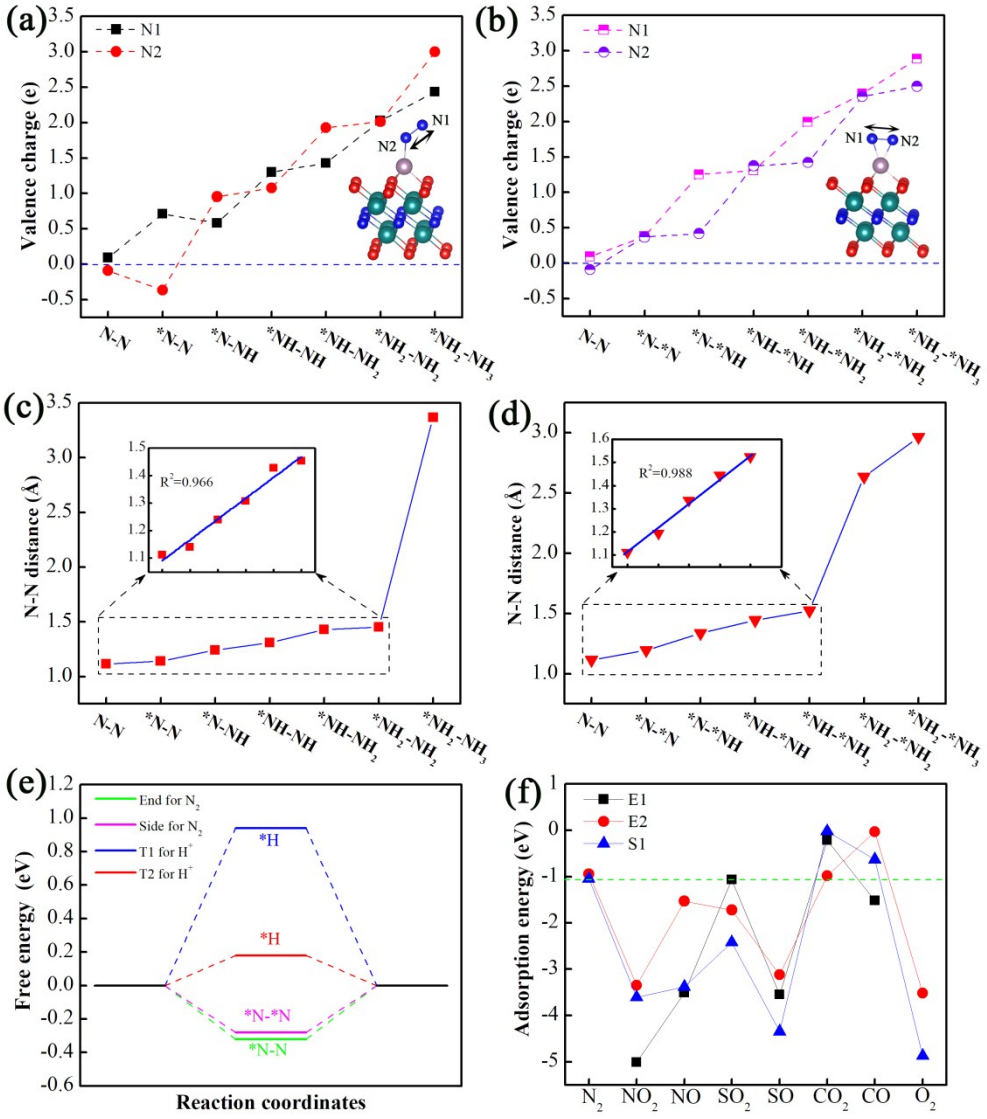

Figure 5. Valence charges of intermediates during NRR on Mo/Ti_2NO_2 surface via (a) end-on and (b) side-on adsorption styles, the N−N bonds length of intermediates during NRR via (c) end-on and (d) side-on adsorptions, where the bond length increases linearly before N_2 was broken, (e) reaction Gibbs free energies of hydrogen (H^+) and N_2 adsorption, and (f) the adsorption energies of potential extra gas on Mo/Ti_2NO_2 surface.

The quantitative charge transfers of intermediates based on Bader charge analysis are shown in Figures 5a and b and Table S10. For an isolated N_2 molecule, the two N atoms gain or lose 0.091*e*, respectively. The N_2 gains 0.34*e* and 0.52*e* when adsorbed on Mo/Ti_2NO_2 surface via the end-on and side-on configurations, respectively. The more thoroughly is the NRR on catalyst surface, the higher valence charges of N in $*N_2H_y$. For example, the valence charges of two N atoms are 1.25 and 0.44 *e* in *N-*NH species, respectively, while these values are 2.38 and 2.41 *e* in $*NH_2$-$*NH_2$ species. The bond lengths present a linearly increasing from N_2 molecule to $*NH_2$-

NH_2 (Figure 5c) and *NH-*NH_2 (Figure 5d), indicating that the gradual stretching with hydrogenation. Moreover, the valence charges of N approach to 3*e* when hydrogenation to *NH_2-*NH_3 (*NH_2-NH_3), and the corresponding N-N bond lengths are approximately to 3.0Å, indicating that the NH_3 will form and release from Mo/Ti_2NO_2 surface. The results of valence charges and N−N bond lengths of intermediates of NRR on Mo/V_2NO_2 and Mo/Cr_2NO_2 surfaces are shown in Figures S14 and S15. Results show that they have similar charge transfer trends with that of Mo/Ti_2NO_2. However, the higher η_{NRR} restricts the NRR performances of Mo/V_2NO_2 and Mo/Cr_2NO_2. Therefore, Mo/Ti_2NO_2 is the best efficient catalyst for electrochemical NRR among studied TM/M_2CO_2. One should note that the energies of the final state in Figures 3, S4, S5, S9 and S10 are different. The reason caused such results is that the energy of the initial state (+N_2) is catalyst dependent, but was set to be zero as a reference for all reactions for comparison.

Potential side reactions on Mo/Ti_2NO_2 surface

Theoretically, the active sites of Mo/Ti_2NO_2 can be occupied immediately by N_2 to form *N_2 once NH_3 desorbing from Mo/Ti_2NO_2 surface. However, if there are sufficient protons (H^+) in the vicinity of the active sites of Mo/Ti_2NO_2, the H^+ will be adsorbed on the surface and the hydrogen evolution reaction (HER) will be occurred, which will poison the active sites of Mo/Ti_2NO_2 surface and lower the efficiency of NRR.[71, 72] On the other hand, the catalyst can also be poisoned if extra gases mixed in the N_2 source (such as CO_2, and O_2) and adsorbed on the active sites of catalyst. Therefore, it is necessary to study the adsorption properties of hydrogen and other gases on the Mo/Ti_2NO_2 surface to evaluate its resistance ability to be poisoned. There are two different sites for H adsorption, T1 and T2 sites, as schematically are shown in Figure S16. The Gibbs free energy of hydrogen adsorption (ΔG_{H*}) on Mo/Ti_2NO_2 are shown in Figure 5e. It shows that ΔG_{H*} are 0.94 and 0.18 eV, respectively, for T1 and T2 sites with the corresponding overpotentials of 0.94 and 0.18 V, which are larger than that of NRR (0.16 and 0.17 V for end-on and side-on adsorptions, respectively). This result suggests that Mo/Ti_2NO_2 substrate is not in favor for the hydrogen adsorption. For multi-atom molecules (NO, NO_2, SO_2, SO, CO, and NO_2), there are three potential adsorption ways labeled as E1, E2 and S1 (Figure S17), respectively. There are two adsorption styles of O_2, labeled as E2 and S1, respectively. The adsorption energies of gas molecules (including NO, NO_2, SO_2, SO, CO, NO_2, and O_2) on Mo/Ti_2NO_2 surface is evaluated via eq (2) and results are shown in Figure 5f. The adsorption energies of CO_2 with three adsorptions and CO with E2 and S1 sites are larger (higher than -1.05 eV) than that of N_2 adsorption, while the corresponding values of other gases (NO_2, NO, SO_2, SO, and O_2) are lower than that of N_2 adsorption. These results indicate that the bonding strength between the adsorbed

gas molecules (NO_2, NO, SO_2, SO, and O_2) and Mo/Ti_2NO_2 surface are stronger than that between N_2 and Mo/Ti_2NO_2 surface except CO_2 and CO at E2 and S1 sites. The stronger bonding strength of these gas molecules could erode the active sites of Mo/Ti_2NO_2, leading to the poison of Mo/Ti_2NO_2 surface for NRR. Thus, it should be avoided mixing of the gas molecules such as NO_2, NO, SO_2, SO, and O_2 in N_2 source for NRR on Mo/Ti_2NO_2 surface according to this studied results.

Conclusions

In summary, we performed density functional theory calculations to predict the catalytic performances of single TM atom anchored on the 2D M_2NO_2 surface for electrochemical N_2 reduction into NH_3. Results show that the bonding strength between Mo atom and M_2NO_2 is strong. The adsorption energy of N_2 on Mo/Ti_2NO_2 is -1.05 eV via the side-on configuration. Mo/Ti_2NO_2 exhibits an excellent performance via enzymatic mechanism with overpotential of only 0.16 V among studied TM/M_2NO_2. In addition, Gibbs reaction free energy of the NH_3 desorption from Mo/Ti_2NO_2 is ΔG=0.12 eV, implying that NH_3 can be easily released. Moreover, the metallic characteristics of Mo/Ti_2NO_2 will ensure the efficiency of electrons transferring between Mo and Ti_2NO_2 as well. AIMD results indicate that Mo atom can be stably anchored on Ti_2NO_2 substrate to prevent its aggregation into Mo clusters. Further analysis shows that hydrogen adsorption is not in favor on the Mo/Ti_2NO_2 surface, and it should be avoided mixing the gases such as NO_2, NO, SO_2, SO, and O_2 in N_2 source for NRR. The low overpotential for NRR, rapid desorption of NH_3, and excellent electrical conductivity can ensure Mo/Ti_2NO_2 as an efficient catalyst for electrochemical NRR.

Conflicts of interest

The authors declare no competing financial interest.

Acknowledgements

This work was financially supported by the Natural Science Foundation of Shandong, China, Grant No. ZR2014EMM013 and No.ZR2014EMQ009, and the Fundamental Research Funds for the Central Universities Grant No.HIT.KITP.2014030. This work was carried out at LvLiang Cloud Computing Center of China, and the calculations were performed on TianHe-2.

References

1 J. W. Erisman, M. A. Sutton, J. Galloway, Z. Klimont and W. Winiwarter, *Nat. Geosci*., 2008,

1, 636.
2 R. Schlögl, *Angew. Chem. Int. Ed*., 2003, **42**, 2004–2008.
3 J. N. Galloway, A. R. Townsend, J. W. Erisman, M. Bekunda, Z. Cai, J. R. Freney, L. A. Martinelli, S. P. Seitzinger and M. A. Sutton, *Science*, 2008, **320**, 889–892.
4 D. E. Canfield, A. N. Glazer and P. G. Falkowski, *Science*, 2010, **330**, 192–196.
5 A. Fuerte, R. X. Valenzuela, M. J. Escudero and L. Daza, *J. Power Sources*., 2009, 1**92**, 170–174.
6 A. Afif, N. Radenahmad, Q. Cheok, S. Shams, J. H. Kim and A. K. Azad, *Renew. Sust. Energ. Rev*., 2016, **60**, 822–835.
7 V. Rosca, M. Duca, M. T. de Groot and M. T. Koper, *Chem. Rev*.; 2009, **109**, 2209−2244.
8 S. Licht, B. Cui, B. Wang, F. F. Li, J. Lau and S. Liu, *Science*, 2014, **345**, 637−640.
9 M. M. Shi, D. Bao, B. R. Wulan, Y. H. Li, Y. F. Zhang, J. M. Yan and Q. Jiang, *Adv. Mater*., 2017, **29**, No. 1606550.
10 H. Liu, Chin. *J. Catal*., 2014, **35**, 1619–1640.
11 K. M. Lancaster, Y. Hu, U. Bergmann, M. W. Ribbe and S. DeBeer, *J. Am. Chem. Soc*., 2013, **135**, 610−612.
12 J. A. Wiig, Y. Hu, C. C. Lee and M. W. Ribbe, *Science*, 2012, **337**, 1672−1675.
13 R. Dixon and D. Kahn, *Nat. Rev. Microbiol*., 2004, **2**, 621.
14 J. Zhao and Z. Chen, *J. Am. Chem. Soc*., 2017, **139**, 12480−12487.
15 Z. W. Seh, J. Kibsgaard, C. F. Dickens, I. Chorkendorff, J. K. Nørskov and T. F. Jaramillo, *Science*, 2017, **355**, No. eaad4998.
16 X. Cui, C. Tang and Q. Zhang, *Adv. Energy. Mater*., 2018, **8**, 1800369.
17 S. L. Foster, S. I. P. Bakovic, R. D. Duda, S. Maheshwari, R. D. Milton, S. D. Minteer, M. J. Janik, J. N. Renner and L. F. Greenlee, *Nat. Cata*., 2018, **1**, 490–500.
18 C. Guo, J. Ran, A. Vasileff and S.-Z. Qiao, *Energy Environ. Sci*., 2018, **11**, 45–56.
19 L. Yang, T. Wu, R. Zhang, H. Zhou, L. Xia, X. Shi, H. Zheng, Y. Zhang and X. Sun, *Nanoscale*, 2019, **11**, 1555–1562.
20 J. Zhao, L. Zhang, X. Y. Xie, X. Li, Y. Ma, Q. Liu, W. H. Fang, X. Shi, G. Cui and X. Sun, *J. Mater. Chem. A*, 2018, 6, 24031–24035.
21 L. Zhang, X. Ren, Y. Luo, X. Shi, A. M. Asiri, T. Li and X. Sun, *Chem. Commun*., 2018, **54**, 12966–12969.
22 X. Ren, J. Zhao, Q. Wei, Y. Ma, H. Guo, Q. Liu, Y. Wang, G. Cui, A. M. Asiri, B. Li, B. Tang andX. Sun, *ACS Cent. Sci*. 2019, **5**, 116–121.
23 T. Wu, W. Kong, Y. Zhang, Z. Xing, J. Zhao, T. Wang, X. Shi, Y. Luo and X. Sun, *Small Methods*. 2019, 1900356.
24 Y. Abghoui and E. Skulason, *Catal. Today*, 2017, **286**, 78−84.
25 X. Zhang, D. F. Wu and D. J. Cheng, *Electrochim. Acta*, 2017, **246**, 572−579.
26 H. L. Dong, Y. Y. Li and D. E. Jiang, *J. Phys. Chem. C*, **2018**, 122, 11392−11398.
27 A. B. Hoskuldsson, Y. Abghoui, A. B. Gunnarsdottir and E. Skulason, *ACS Sustain. Chem. Eng.*, 2017, **5**, 10327−10333.
28 J. Li, H. Zhou, H. Zhuo, Z. Wei, G. Zhuang, X. Zhong, S. Deng, X. Li and J. Wang, *J. Mater. Chem. A*, 2018, **6**, 2264−2272
29 G. F. Chen, X. Cao, S. Wu, X. Zeng, L. X. Ding, M. Zhu and H. Wang, *J. Am. Chem. Soc.*, 2017, **139**, 9771−9774.

30 L. Fan, P. F. Liu, X. Yan, L. Gu, Z. Z. Yang, H. G. Yang, S. Qiu and X. Yao, *Nat. Commun*., 2016, **7**, No. 10667.
31 Q. Cheng, L. Yang, L. Zou, Z. Zou, C. Chen, Z. Hu and H. Yang, *ACS Catal*., 2017, **7**, 6864−6871.
32 L. Zhang, Y. Jia, G. Gao, X. Yan, N. Chen, J. Chen, M. T. Soo, B. Wood, D. Yang, A. Du and Y. D. Yao, *Chem*, 2018, **4**, 285−297.
33 C. Y. Ling, X. H. Niu, Q. Li, A. J. Du and J. L. Wang, *J. Am. Chem. Soc.*, 2018, **140**, 14161−14168.
34 S. Ji, Z. X. Wang and J. X. Zhao. *J. Mater. Chem. A*, 2019, **7**, 2392-2399.
35 F. Chen, X. Jiang, L. Zhang, R. Lang and B. Qiao, *Chin. J. Catal.*, 2018, **39**, 893−898.
36 S. Back, J. Lim, N. Y. Kim, Y. H. Kim and Y. Jung, *Chem. Sci.*, 2017, **8**, 1090−1096.
37 M. Naguib, M. Kurtoglu, V. Presser, J. Lu, J. Niu, M. Heon, L. Hultman, Y. Gogotsi and M. W. Barsoum, *Adv. Mater*., 2011, **23**, 4248–4253.
38 M. Naguib, O. Mashtalir, J. Carle, V. Presser, J. Lu, L. Hultman, Y. Gogotsi and M. W. Barsoum, *ACS Nano*, 2012, **6**, 1322–1331.
39 M. Naguib, V. N. Mochalin, M. W. Barsoum and Y. Gogotsi, *Adv. Mater*., 2014, **26**, 992–1005.
40 M. Ghidiu, M. R. Lukatskaya, M. Q. Zhao, Y. Gogotsi and M. W. Barsoum, *Nature*, 2014, **516**, 78–81.
41 B. Anasori, M. R. Lukatskaya and Y. Gogotsi, *Nat. Rev. Mater*., 2017, **2**, 16098.
42 N. K. Chaudhari, H. Jin, B. Kim, S. D. Baek, S. H. Joo and K. Lee, *J. Mater. Chem. A*, 2017, **5**, 24564–24579.
43 M. Shao, Y. Shao, W. Chen, K. L. Ao, R. Tong, Q. Zhu, I. N. Chan, W. F. Ip, X. Shi and H. Pan, *Phys. Chem. Chem. Phys*., 2018, **20,** 14504–14512.
44 Y. Gao, Y. Cao, H. Zhuo, X. Sun, Y. Gu, G. Zhuang, S. Deng, X. Zhong, Z. Wei, X. Li and J. Wang, Catal. Today, 2018, 10.1016/j.cattod.2018.12.029.
45 R. P. Pandey, K. Rasool, V. E. Madhavan, B. Aissa, Y. Gogotsi and K. A. Mahmoud, *J. Mater. Chem. A*, 2018, **6**, 3522−3533.
46 L. Lorencova, T. Bertok, J. Filip, M. Jerigova, D. Velic, P. Kasak, K. A. Mahmoud and J. Tkac, *Sensors Actuat. B*, 2018, **263**, 360−368.
47 B. B. Cui, B. Hu, J. M. Liu, M. H. Wang, Y. P. Song, K. Tian, Z. H. Zhang and L. H. He, *ACS Appl. Mater. Interfaces.*, 2018, **10**, 23858–23873.
48 B. M. Hoffman, D. R. Dean and L. C. Seefeldt, *Acc. Chem. Res*., 2009, **42**, 609–619.
49 D. V. Yandulov and R. R. Schrock, *Science*, 2003, **301**, 76–78
50 C. Y. Ling, X. W. Bai, Y. X. Ouyang, A. J. Du, and J. L. Wang, *J. Phys. Chem. C*, 2018, **122**, 16842−16847.
51 Y. J. Gao, H. Zhuo, Y. Y. Cao, X. Sun, G. L. Zhuang, S. W. Deng, X. Zhong, Z. Z. Wei, Jianguo Wang. Chin. *J. Catal*., 2019, **40**, 152–159.
52 Q. Li, L. He, C. Sun and X. Zhang, *J. Phys. Chem. C*, 2017, 121, 27563–27568.
53 H. Cheng, L. X. Ding, G. F. Chen, L. Zhang, J. Xue and H. Wang, *Adv. Mater.*, 2018, 30, e1803694.
54 P. Ou, X. Zhou, F. Meng, C. Chen, Y. Chen, and J. Song, *Nanoscale*, 2019,11, 13600-13611.
55 G. Kresse and J. Furthmüller, *Comput. Mater. Sci.*, 1996, **6**, 15−50.
56 G. Kresse and J. Furthmüller, *Phys. Rev B: Condens. Matter Mater. Phys*., 1996, **54**,

11169−11186.
57 J. P. Perdew, J. A. Chevary, S. H. Vosko, K. A. Jackson, M. R. Pederson, D. J. Singh and C. Fiolhais, *Phys. Rev. B: Condens. Matter Mater. Phys*., 1992, **46**, 6671–6687.
58 J. P. Perdew, K. Burke and M. Ernzerhof, *Phys. Rev. Lett*., 1996, **77**, 3865-3868.
59 G. Kresse and D. Joubert, *Phys. Rev B: Condens. Matter Mater. Phys*., 1999, **59**, 1758-1775.
60 S. Grimme, J. Antony, S. Ehrlich and S. Krieg, *J. Chem. Phys*., 2010,**132**, 154104.
61 J. Rossmeisl, A. Logadottir and J. K. Nørskov, *Chem. Phys.*, 2005, **319**, 178−184.
62 A. A. Peterson, F. Abild-Pedersen, F. Studt, J. Rossmeisl and J. K. Nørskov, *Energy Environ. Sci.*, 2010, **3**, 1311−1315.
63 Y. W. Cheng, J. H. Dai, Y. M. Zhang and Yan Song, *J. Phys. Chem. C*, 2018, **122**, 28113−28122.
64 L. Li, B. Li, Q. Guo and B. Li, *J. Phys. Chem. C*, 2019, **123**, 14501−14507.
65 J. Zhang, Y. Zhao, X. Guo, C. Chen, C. L. Dong, R. S. Liu, C. P. Han, Y. Li, Y. Gogotsi and G. Wang, *Nat. Catal*, 2018, **1**, 985–992.
66 L. Li , X. Wang, H. Guo, G. Yao, H. Yu, Z. Tian , B. Li, L. Chen, *Small Methods*, 2019, 1900337.
67 G. Henkelman, A. Arnaldsson and H. Jonsson, *Comput. Mater. Sci.*, 2006, **36**, 354−360.
68 E. Skúlason, T. Bligaard, S. Gudmundsdóttir, F. Studt, J. Rossmeisl, F. Abild-Pedersen, T. Vegge, H. Jónsson and J. K. Nørskov, *Phys. Chem. Chem. Phys.*, 2012, **14**, 1235−1245.
69 L. M. Azofra, N. Li, D. R. MacFarlane and C. Sun, *Energy Environ. Sci*., 2016, **9**, 2545−2549.
70 H. R. Zhu, Y. L. Hu, S. H. Wei and D. Y. Hua, *J. Phys. Chem. C*, 2019, **123**, 4274–4281.
71 A. R. Singh, B. A. Rohr, J. A. Schwalbe, M. Cargnello, K. Chan, T. F. Jaramillo, I. Chorkendorff and J. K. Nørskov, *ACS Catal.*, 2017, **7**, 706–709.
72 Y. C. Hao, Y. Guo, L. W. Chen, M. Shu, X. Y. Wang, T. A. Bu, W. Y. Gao, N. Zhang, X. Su, X. Feng, J. W. Zhou, B. Wang, C. W. Hu, A. X. Yin, R. Si, Y. W. Zhang and C. H. Yan, *Nat. Cata.*, 2019, **2**, 448–456.

Table of content

Mo anchored on Ti_2NO_2 (Mo/Ti_2NO_2) surface possesses superior NRR performances, with the overpopential η_{NRR} of 0.16 V via enzymatic mechanism.